ELSEVIER

Contents lists available at ScienceDirect

Materialia

journal homepage: www.elsevier.com/locate/mtla



Full Length Article

Core structure and mobility of edge dislocations in face-centered-cubic chemically complex NiCoFe and NiCoFeCu equiatomic solid-solution alloys



Wei Li^{a,b,c}, Satish I. Rao^a, Qingyuan Wang^b, Haidong Fan^b, Junjie Yang^a, Jaafar A. El-Awady^{a,*}

- a Department of Mechanical Engineering, Whiting School of Engineering, The Johns Hopkins University, Baltimore, MD 21218, United States
- b MOE Key Laboratory of Deep Earth Science and Engineering, College of Architecture and Environment, Sichuan University, Chengdu 610065, China
- ^c Department of Engineering Mechanics, Chongqing University, Chongqing 400044, China

ARTICLE INFO

Keywords: Equiatomic solid-solution alloys High entropy alloys Dislocation core structure Critical resolved shear stress Chemically complex alloys

ABSTRACT

The elastic properties, core structures, critical resolved shear stresses (CRSSs), and mobility of $1/2\langle110\rangle$ edge dislocations in NiCoFe and NiCoFeCu equiatomic solid-solution alloys was predicted using molecular statics and dynamics simulations using two different embedded atom method (EAM) potentials. In particular, the Johnshon–Zhou potential is in good agreement with experimental measurements and observations. The calculated average intrinsic stacking fault energies for both alloys were 17 and 28 mJ/m², and the mean stacking fault width in the absence of external stresses were 70 and 51 Å, respectively. The CRSSs for both alloys were between 50–60, 40–50, and 30–40 MPa at 10, 150, and 300 K, respectively. These results are in reasonable agreement with available experimental measurements and theoretical predictions. The atomistic simulations presented here can be used to predict and develop face-centered cubic chemically complex alloys with superior strength for various applications.

Chemically complex solid-solution alloys, multi-component alloys having high concentrations of individual solutes, are of significant interest due to their excellent mechanical properties. Single phase face-centered cubic (FCC) equiatomic solid-solution alloys exhibit high tensile strength, ductility, and remarkable fracture toughness at low temperatures [1-3]. The initial stages of plastic deformation in FCC equiatomic solid-solution alloys is entirely accommodated by dislocation slip [4,5], whereas deformation twins are observed at higher plastic strains [4,6]. TEM observations of CoCrFeMnNi alloy strained to 2% at 77, 293 and 873 K indicate that plasticity is accommodated by $1/2\langle 110 \rangle$ dislocations on {111} planes, and numerous stacking faults (SFs) and dislocation multipoles were also observed [4]. The separation of Shockley partials of a 1/2(110) 60° dislocation in CoCrFeMnNi alloy was also experimentally measured and showed significant variations along the dislocation line, from 1-9 nm, and the average stacking fault energy (SFE) measured was $\sim 30 \text{ mJ/m}^2$ [7]. Atomistic simulations also showed core structure variations for 1/2[110] screw and edge dislocations in FCC $\mathrm{Co_{30}Fe_{16.67}Ni_{36.67}Ti_{16.67}}$ as well as in 1/2[111] screw dislocation in body centered cubic (BCC) $\mathrm{Co}_{16.67}\mathrm{Fe}_{36.67}\mathrm{Ni}_{16.67}\mathrm{Ti}_{30}$ alloys [8,9].

Although recent studies have shown that solute strengthening is mainly responsible for the high yield strength of FCC and BCC concentrated solid-solution alloys [10–13], it is different from conventional solid-solution hardening in dilute alloys due to the high concentration of solutes in these alloys. Theoretical models of solid-solution strength-

ening in concentrated FCC and BCC alloys were recently developed based on an average effective medium corresponding to the alloy composition and treating the interaction of individual solutes with an edge dislocation core in this medium [10–13]. The effective medium concept was also used to model solid-solution strengthening in concentrated BCC alloys using the Suzuki model and yielding dominated by screw dislocations [14,15]. However, these models require the calculation of solute-dislocation core interaction energies in the effective medium.

Here, we utilize molecular statics (MS) and molecular dynamics (MD) simulations using embedded-atom method (EAM) potentials for calculating the critical stress and mobility of $1/2\langle110\rangle$ edge dislocations in face-centered cubic equiatomic NiCoFe and NiCoFeCu alloys at temperatures ranging from 0–300 K. Such simulation results are compared with experimentally measured room temperature yield stresses in these alloys. They are also compared with critical resolved shear stresses for the movement of $1/2\langle110\rangle$ edge dislocations at 0 K obtained by the reduced misfit solution strengthening theory.

All atomistic simulations here were conducted using the parallel MD simulator, LAMMPS [16]. The four-element Ni-Co-Fe-Cu interatomic potential developed by Zhou et al. [17] (hereafter referred to as the Johnsons–Zhou potential) was adopted to describe the interatomic interactions in the studied alloys. The Johnsons–Zhou potential was developed by fitting to experimental equilibrium crystal structure, co-hesive energy, vacancy formation energy, lattice constants, and elastic

E-mail address: jelawady@jhu.edu (J.A. El-Awady).

^{*} Corresponding author.

Table 1

Lattice parameter (Å) and elastic constants (GPa) as predicted using the Johnson–Zhou potential (EAM¹) and the Farkas–Caro potential (EAM²) for Ni, NiCoFe, and NiCoFeCu.

Materials	Α		C_{11}		C_{12}		C_{44}		(C11-C12)/2		A		$G_{\{111\}}$	G_V	G_R	$G_{V\!RH}$
	EAM ¹	EAM ²	EAM^1	EAM^1	EAM^1	EAM^1										
Ni	3.515	3.515	247	248	147	148	125	125	50	50	2.5	2.5	78.7	94.7	77.8	86.2
NiCoFe	3.545	3.545	183	263	141	165	107	119	21	49	5.1	2.4	47.4	72.6	40.6	56.6
NiCoFeCu	3.578	3.558	173	228	125	146	101	106	24	41	4.2	2.6	49.2	70.2	44.2	57.2

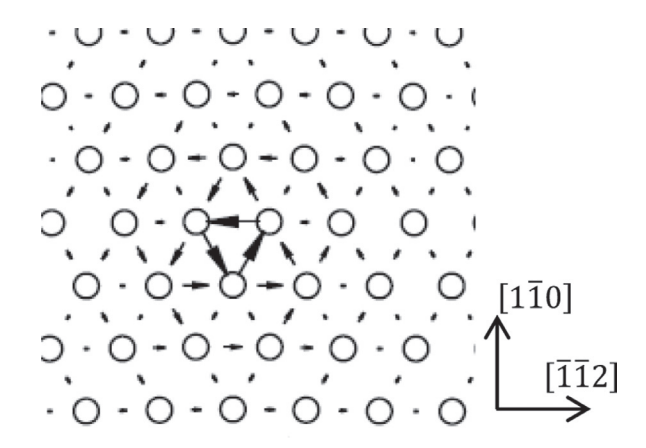


Fig. 1. Differential displacement plot of the core structure of a 1/2[111] screw dislocation in BCC Fe as obtained using the Johnsons–Zhou potential. The core structure obtained compares favorably with first principles results [19].

constants for the pure elements, Ni, Co, Fe, and Cu [17]. The Ni, Co, and Cu potentials also give stacking fault energy in reasonable agreement with available experimental data. The stacking fault energy given by the Johnsons–Zhou potential for Ni was evaluated in this study and is $\sim 100 \text{ mJ/m}^2$ in agreement with an experimental result of $\sim 120 \text{ mJ/m}^2$ [18]. Also, the core structure of 1/2[111] screw dislocations in BCC Fe was as evaluated using the Zhou potential gives a compact core structure (see Fig.1), which is in agreement with first principles results [19].

Additionally, for comparison purposes, simulations are also conducted using the newly develop Farkas–Caro EAM potential [20]. This potential was developed to resemble but not precisely model near-equiatomic mixtures of Fe–Ni–Cr–Co–Cu [20].

For the analysis, the local lattice and defect structures were quantified using the common neighbor analysis (CNA) [21] and the centro-symmetric parameter (CSP), respectively, whereas visualization of the atomistic structures was performed using OVITO [22].

All simulations were performed on rectangular simulation cells constructed by randomly distributing Ni, Co, Fe (and Cu) atoms with equal concentrations as a representative model for NiCoFe (and NiCoFeCu). The average lattice constants of both alloys were first computed by generating cubic simulation cells having edge-length ~300 Å and edges oriented parallel to the X-[100], Y-[010], and Z-[001] crystallographic directions. Periodic boundary conditions (PBC) were employed along all three orthogonal directions and the total number of atoms were ~2 million. The average lattice constants at 0 K corresponding to the minimum cohesive energy after energy minimization by the conjugate gradient (CG) algorithm for NiCoFe and NiCoFeCu were 3.545 and 3.578 Å, respectively, with either potentials. These values agree well with experimental measurements at room temperature of both alloys (i.e. 3.557 and 3.586 Å, respectively [23]).

The elastic constants were also calculated by straining the defect-free lattice with the minimum cohesive energy at 0 K. The predicted elastic constants are summarized in Table 1 for both EAM potentials, which meet the Born stability criteria (i.e. $C_{11} + 2C_{12} > 0$; $C_{11} - C_{12} > 0$ and $C_{44} > 0$) [24]. As shown in Table 1,

the anisotropy ratios, $A=2C_{44}/(C_{11}-C_{12})$, for Ni, NiCoFe, and NiCoFeCu are much larger than one, indicating all three compositions are being of high elastic anisotropy. The shear moduli in the $\langle 110 \rangle$ direction of $\{111\}$ plane, $G_{\{111\}}=[(C_{44}(C_{11}-C_{12})/2]^{1/2}]$, are also listed in Table 1. Since Ni and both alloys have high elastic anisotropy, the Voigt and Reuss average shear moduli, G_V and G_R , are also shown in Table 1 and they provide an upper and lower shear modulus bounds, respectively, for polycrystals [25]. Additionally, the Voigt–Reuss–Hill arithmetic average shear modulus, G_{VRH} [26], is also given in Table 1. It should be noted that G_{11} as predicted using the Farkas–Caro potential is 30–40% higher as compared to that predicted from the Johnson-Zhou potential, whereas the predicted G_{12} using the Farkas–Caro is 15–20% higher. The G_{44} predicted from both potentials are similar.

The average SFE determines the width of core splitting of $1/2\langle 110\rangle$ dislocations in FCC crystals. The SFE of Ni, NiCoFe, and NiCoFeCu were calculated using MS simulations of rectangular cells having edge lengths $60\sqrt{3/2}a$, $60\sqrt{2}a$, and $60\sqrt{3}a$ along the X-[11 $\bar{2}$], Y-[$\bar{1}10$], and Z-[111], respectively. PBCs were employed along the [11 $\bar{2}$] and [$\bar{1}10$] directions, whereas free boundary conditions were employed along the [111] direction. The intrinsic SFE was obtained by displacing the upper half in the 'z' direction of the crystal relative to the bottom half along the SF vector and relaxing using CG energy minimization from the displaced position.

The calculated unstable SFE, γ_{us} , and the intrinsic stacking fault (ISF) energy, γ_{isf} , for Ni, NiCoFe and NiCoFeCu are summarized in Table 2 for both potentials. It is clear that γ_{isf} for both alloys as predicted from both potentials is much smaller than that of pure Ni. For comparison purposes, γ_{isf} of other FCC equiatomic solid-solution alloys, such as, NiCoCr (18–26 mJ/m² [27]), NiFeCrCo (20 mJ/m² [28]), and NiFeCrCoMn, (25 mJ/m² [28]) are also low relative to pure Ni.

Additionally, the predicted γ_{isf} for Ni from both potentials is within ~10% of that measured from XRD experiments (108 mJ/ m^2) [29]. However, using the Johnson–Zhou potential, γ_{isf} for NiCoFe was 45% smaller than that measured for the same alloy from XRD experiments (31 mJ/ m^2), and that predicted using the Farkas–Caro potential is more than double the experimental measurement. Also, the shear modulus $G_{\{111\}}$ as predicted from the current simulations using the Johnson–Zhou potential for NiCoFe is 24% smaller as compared to that obtained experimentally (62 GPa) [29], and 24% higher when using the Farkas–Caro potential.

In order to calculate the core structure of $1/2\langle 110 \rangle$ edge dislocations and their CRSS, an edge dislocation was introduced into the center of a rectangular simulation cell having edges parallel to the X-[110], Y-[112], and Z-[111] crystallographic directions. The CRSS is defined here as the stress at which the dislocation would completely overcome the solute obstacles and continuously glide to accommodate the imposed plastic deformation. The edge dislocation was introduced into the simulation cell using its anisotropic elasticity displacement field, then a complete relaxation using CG minimization was performed. The dislocation line direction was along the Y-[112] direction, and the glide plane normal was in the Z-[111] direction. PBCs were employed along the [112] direction (i.e. parallel to dislocation line) and [110] direction (i.e. parallel to the glide direction), whereas free boundary conditions were imposed along the [111] direction. To minimize the effects of image forces arising from image dislocations and free surfaces, the edge lengths of the simulation cell in the X, Y, and Z directions were 120, 60, and

Table 2
The SFE (mJ/m^2), and the minimum, maximum, and mean SF width (Å), as obtained from MS simulations for Ni, NiCoFe and NiCoFeCu. For comparison, published experimental measurements, and predictions from the anistropic elasticity theory are also included. The predictions were made using both the Johnson–Zhou potentials (EAM 1) and the Farkas-Caro potential (EAM 2).

Materials	γ_{us}		γ_{isf}		γ^e_{isf}	w _{min}		W _{max}		W _{mean}		W _{aniso}	
	EAM ¹	EAM ²	EAM ¹	EAM ²		EAM ¹	EAM ²	EAM ¹	EAM ²	EAM ¹	EAM ²	EAM ¹	EAM ²
Ni	252	366	98	120	108 [24]	22	24	22	24	22	24	24	24
NiCoFe	114	294	17	67	31 [24]	53	31	97	39	70	34	109	37
NiCoFeCu	129	273	28	66	-	44	24	63	40	51	32	65	33

30 nm, respectively. The total number of atoms in the simulation cell was \sim 20 million atoms. The simulation cells were heated up to three temperatures (10, 150, and 300 K) using the velocity Verlet algorithm, then relaxed under the desired temperature with the NVT ensemble for 50 ps to reach thermal equilibrium. External forces were imposed on all atoms in two thin slabs (thickness of each slab is 1.2 nm) at the surfaces of the simulation cell in the Z direction to produce the desired shear stress. Additionally, the whole simulation cell was linearly strained corresponding to the applied stresses at the onset of loading to eliminate inertial effects. Such a cell was then relaxed using an NVT thermostat at 10, 150, and 300 K for 350, 700, and 800 ps, respectively [8].

The completely relaxed core structures of edge dislocations in both alloys using the Johnson–Zhou potential are shown at 0 ps in Fig. 2(a), (c), and (e) at 10, 150, and 300 K, respectively. The core structures of the dislocations in both alloys are similar to that in classical pure Ni crystals. The dislocation core is planar, consisting of a pair of Shockley partials bounding a SF and, which is spread out on {111} glide plane. However, unlike in a pure Ni crystal, the SF widths in both alloys were observed to vary significantly along the dislocation line rather than remain constant due to the local fluctuations of SFE induced by fluctuations in the local concentration in both equiatomic solid-solution alloys. This is in good qualitative agreement with experimental observations in other HEA (cf. CrMnFeCoNi [7]). Throughout the dislocation glide process, the SF width varies considerably for both alloys as shown in Fig. 2(a), (c), and (e). Additionally, the mean SF width in NiCoFe is slightly larger than that in NiCoFeCu.

The mean, minimum, and maximum SF widths under stress-free conditions in Ni, NiCoFe and NiCoFeCu are summarized in Table 2 as predicted using both potentials. While both potentials predict larger SF widths for NiCoFe and NiCoFeCu as compared to pure Ni, those predicted from Johnson–Zhou potential predicts are larger than those predicted from the Farkas–Caro potential. This is due to the much larger γ_{isf} predicted by the Farkas–Caro potential. On the other hand, the results predicted by the Johnson–Zhou potential are more in line with the experimental predictions.

The anisotropic elasticity estimate [30] of the average SF width, w_{aniso} , for edge dislocations in pure Ni, NiCoFe, and NiCoFeCu are also listed in Table 2 for comparison. It is clear that the SF width from theoretical predictions are in approximate agreement (within 10–30%) with that from MS simulations for Ni, NiCoFe, and NiCoFeCu alloys using both potentials. Nevertheless, it should be noted that, anisotropic elasticity predictions assume a straight dislocation and no lattice forces. In these alloys, due to the variations along the dislocation line of Shockley partial splitting, there are line tension forces at equilibrium. In addition, under zero stress, the dislocation experiences solid-solution strengthening forces when relaxed at equilibrium. Therefore, the above effects cause the calculated splitting widths from atomistic simulations to be slightly different from the simple anisotropic elasticity predictions.

Fig. 2(b), (d), and (f) show the mean dislocation position with respect to the cell surface in the $X-[1\bar{1}0]$ direction as a function of time and temperature in both NiCoFe and NiCoFeCu under different applied stresses using the Johnson–Zhou potential. In both alloys the dislocation is immobile under an applied constant shear stress of 50 MPa at 10 K, and 30 MPa at 150 and 300 K for the duration of the simulations. On

the other hand, both dislocations continuously glide until each reaches the simulation cell free surface under constant shear stresses of 60 MPa at 10 K, 50 MPa at 150 K, and 40 MPa at 300 K, respectively. At 150 K and under a constant shear stresses of 40 MPa, the dislocation glides a short distance, then stops for the remainder of the simulation time as shown in the inset of Fig. 2(d).

It should be noted that due to the random nature of atom distributions in both alloys, the solid solution energy barrier that the dislocation has to overcome for motion varies as the dislocation moves. In these simulations, after a short movement, if the solid solution energy barrier is too high for the dislocation to overcome the applied stress the dislocation will stop. This is a main reason why, in these alloys, the dislocation motion has to occur over large distances before one can be confident that the energy barrier spectrum has been reasonably sampled and the critical stress for the movement of dislocations has been measured. The CRSSs for the motion of $1/2\langle 110 \rangle$ edge dislocations of both alloys are summarized as a function of temperature in Fig. 3.

The CRSS calculations were repeated using three random seeds to construct the random distribution of atoms in the simulation cell. Similarly, the simulation time was increased to 1 ns in some simulations. Also, larger cell simulations by increasing the dimension along the dislocation line direction (i.e. 'y' direction) to 120 nm was also performed. The results of all these simulations were very similar with the results shown in Figs. 2 and 3.

The CRSS for both alloys can also be estimated using the simplified elastic misfit solution strengthening model in highly concentrated FCC solid-solution alloys developed by LaRosa et al. [31]. The theoretical CRSS at 0 K is [31]:

$$\tau_{y0} = 0.051 \alpha^{-\frac{1}{3}} \mu \left(\frac{1+v}{1-v}\right)^{\frac{4}{3}} f_1(\omega_c) \times \left[\frac{\sum_n c_n \left(\Delta \bar{V}_n^2 + \sigma_{\Delta V_n}^2\right)}{b^6}\right]^{\frac{2}{3}}$$
(1)

while the energy barrier for dislocation glide is

$$\Delta E_b = 0.274 \alpha^{\frac{1}{3}} \mu b^3 \left(\frac{1+v}{1-v} \right)^{\frac{2}{3}} f_2(\omega_c) \times \left[\frac{\sum_n c_n \left(\Delta \bar{V}_n^2 + \sigma_{\Delta V_n}^2 \right)}{b^6} \right]^{\frac{1}{3}}$$
 (2)

and

$$f_1(\omega_c) = \left[\left(\frac{b}{\omega_c} \right)^{\frac{5}{2}} \sum_{i,j} \Delta f_{ij}^2(\omega_c) \right]^{2/3} \tag{3}$$

$$f_2(\omega_c) = \left[\left(\frac{\omega_c}{b} \right)^2 \sum_{i,j} \Delta f_{ij}^2(\omega_c) \right]^{1/3} \tag{4}$$

Here, $\alpha=0.123$ is a line tension parameter with the line tension $T=\alpha\mu b^2$ [31], μ is taken as $G_{\{111\}}$ or G_V , ν is the Poisson's ratio, ω_c is the amplitude of movement perpendicular to the dislocation line at criticality as the dislocation overcomes the solute obstacle field, $f_1(\omega_c)$ and $f_2(\omega)$ are minimized dislocation core coefficients dependent on the Shockley partials core width [31], c_n and $\Delta \bar{V}_n$ are the concentration and mean misfit volume of the nth solute in the effective medium,

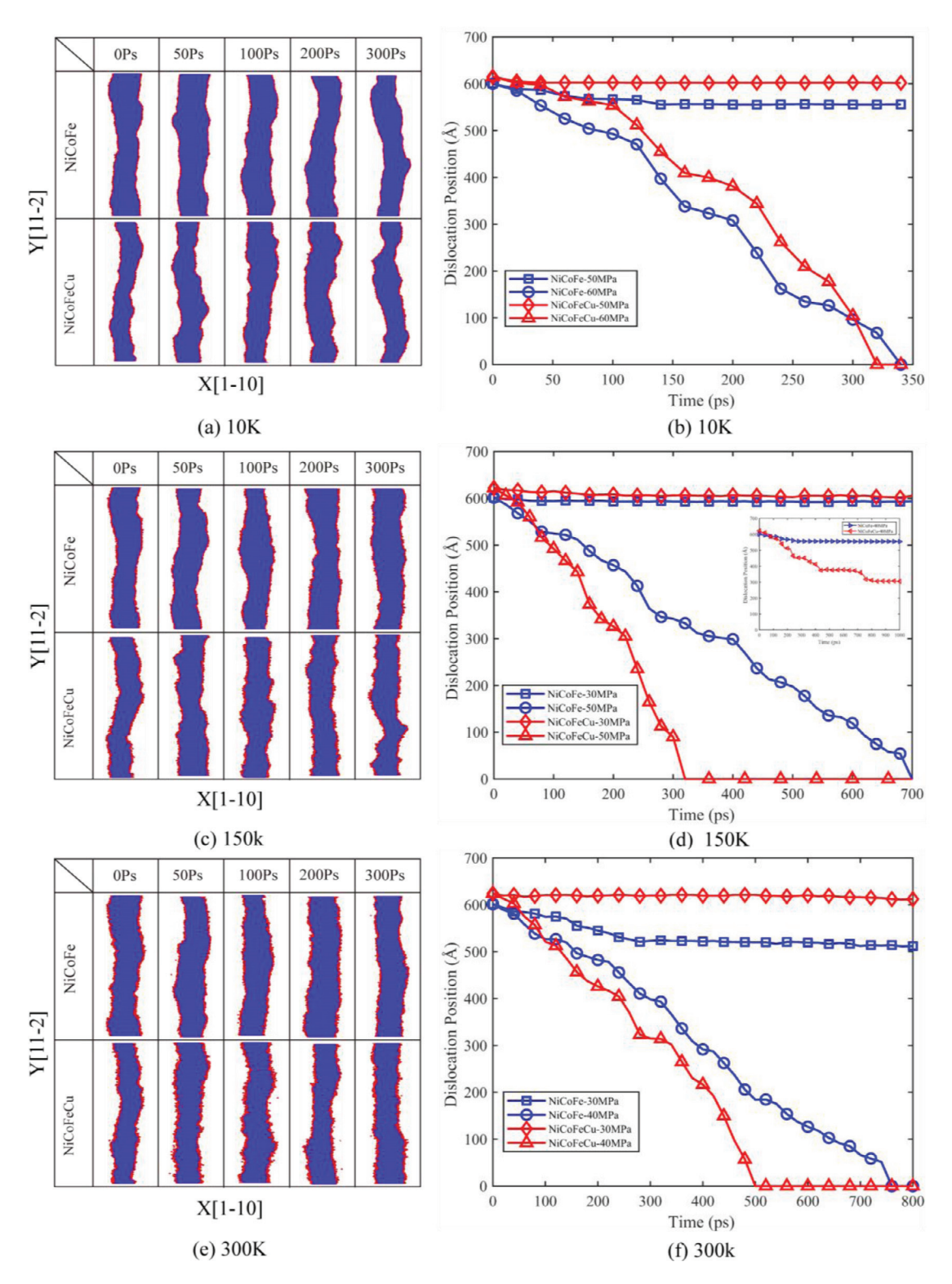


Fig. 2. Dislocation core structures in NiCoFe and NiCoFeCu using the Johnson–Zhou potential during motion at (a) 10 K, (c) 150 K, and (e) 300 K under a resolved shear stress of 60, 50, and 40 MPa, respectively. Red atoms represent the Shockley partial dislocation cores and blue atoms represent the SF. The mean positions of the dislocations as a function of time in NiCoFe and NiCoFeCu under external constant resolved shear stresses are shown at (b) 10 K, (d) 150 K and (f) 300 K. (For interpretation of the references to color in this figure legend, the reader is referred to the web version of this article.)

 $\sigma_{\Delta V_n}$ is its standard deviation in the mean misfit volume and taken to be zero here. For the SF width seen in the simulations for these alloys, $f_1(\omega_{\rm c})\sim 0.2$ and $f_2(\omega_{\rm c})\sim 5.0$ [31]. The various parameters related to -(Eqs. (1)–(4) are summarized in Table 3 for both alloys. The misfit volumes, $\Delta \bar{\rm V}_n$, were obtained from atomistic simulations by

inserting different solutes in the effective medium and determining the corresponding volume change [12]. The theoretical CRSS at 0 K, as predicted from Eq. (1) were 18–28 MPa and 38–54 MPa, whereas the energy barrier for the dislocation to overcome the solute obstacles, were 0.631-0.981 and 0.886-1.259 eV for NiCoFe and NiCoFeCu, respec-

Table 3
The computed quantities related to the elastic misfit solid-solution strengthening model in highly concentrated solid-solution alloys at 0 K. $\Delta \bar{V}_n$ is the mean misfit volume for Ni, Co, Fe, and Cu elements. μ is the shear modulus, ν is Poisson's ratio, b is the Burgers vector, τ_{y0} is critical stress at 0 K, ΔE_b is the energy barrier, σ is the core width of Shockley partial.

Materials	$\Delta \bar{V}_{Ni} \; (\mathring{\rm A}^3)$	$\Delta \bar{V}_{Co} (\mathring{\mathrm{A}}^3)$	$\Delta \bar{V}_{Fe} \; (\mathring{\rm A}^3)$	$\Delta \bar{V}_{Cu} \; (\mathring{\rm A}^3)$	μ (GPa)	ν	b (Å)	σ (Å)	τ_{y0} (MPa)	$\Delta E_b \; (eV)$
NiCoFe	-0.303	-0.115	0.421	-	47.4	0.465	2.51	10.92	18-28	0.631-0.981
NiCoFeCu	-0.614	-0.428	0.466	0.635	49.2	0.432	2.53	9.56	38-54	0.886-1.259

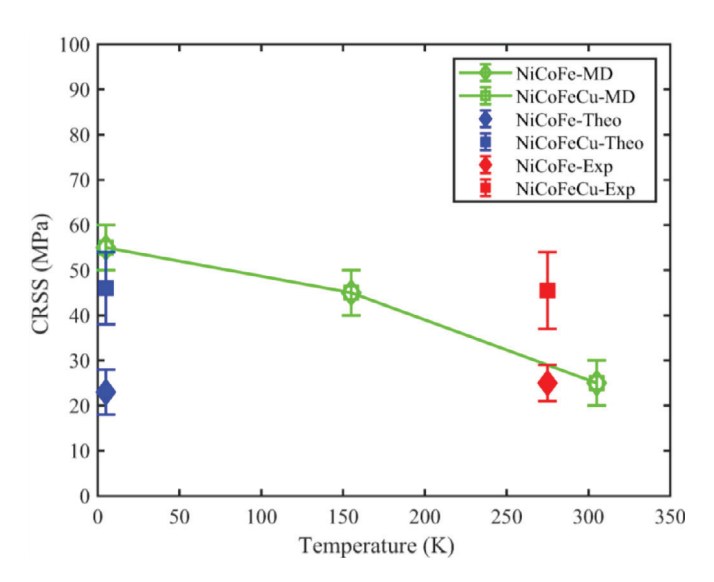


Fig. 3. CRSS of edge dislocations as a function of temperature in NiCoFe and NiCoFeCu alloys, measured from the MD simulations using the Johnson–Zhou potential at 10–300 K and tension experiments at room temperature [32,33]. The theoretical predictions at 0 K are also shown.

tively. These results are also shown in Fig. 3 for easy comparison with the MD predictions at 0 K. It is noted that the theoretical predictions for NiCoFeCu are in good agreement with the MD predictions, however, poor agreement is observed for NiCoFe. While this discrepancy could be due to the potentials used, it should be noted that the theoretical model is a simplified elasticity model, which does not take into account the chemical interaction at the core of the Shockley partials at the edge dislocation properly, and this could be another source of discrepancy between the MD predictions and the theoretical model.

The reported experimental polycrystal yield stress of both alloys at room temperature was corrected by eliminating grain size effects using the classical Hall-Petch relation and was extrapolated to infinite grain sizes to be compared with the current simulations. In the experiments, the grain sizes were about 100 and 20 µm, whereas the yield stresses (at 0.2% plastic strain) were ~125-150 MPa and 250-300 MPa for NiCoFe [32] and NiCoFeCu [33], respectively. The Hall-Petch coefficient for High Entropy alloys is ~ 600 MPa $\mu m^{-0.5}$ [34], for the extrapolation analysis. Finally, in converting yield stresses to CRSS, the experimental yield stresses were divided by the Taylor factor, which is 3.0 for nontextured polycrystals. This analysis results in an estimated CRSS at room temperature of 22-30 MPa and 38-55 MPa for NiCoFe and NiCoFeCu, respectively. These results are also shown in Fig. 2 for easy comparison with the MD predictions at room temperature. The values are in good agreement with the MD predictions for the NiCoFe alloy, whereas in fair agreement for the NiCoFeCu alloy. A possible reason for this discrepancy is that the simulations assumed a completely random solid solution, whereas the real alloys may have some short-range order which may contribute to some strengthening, which have been ignored in the current calculations [35,36].

In summary, two different EAM potentials were utilized to determine the elastic properties, stacking fault widths, and the critical resolved shear stresses required for the sustained motion of $1/2\langle 110 \rangle$ edge dislocations in NiCoFe and NiCoFeCu equiatomic solid-solution alloys at 10-300 K using MS and MD simulations. In particular, the Johnshon-Zhou potential [17] was shown to be in good agreement with experimental measurements and observations. The computed elastic properties agree well with experimental results, whereas the computed stacking fault energies are in fair agreement with experimental results (within 45%). The discrepancies between the simulations and experiments in the determination of stacking fault energy may be attributed to the potential used, assumption of a completely random solid solution [35,36], and/or errors in the interpretation of the x-ray diffraction measurements. The computed stacking fault width was shown to vary considerably along the dislocation line due to local fluctuations in concentration, which agrees well with available experimental data on a fcc high entropy alloy [7]. Finally, the computed critical resolved shear stresses for the movement of a/2<110> edge dislocations as a function of temperature from the current molecular dynamics simulations using the Johnson-Zhou potential for both alloys, compare favorably with experimental measurements as estimated from polycrystals as well as the results from an elastic misfit solid-solution strengthening model at 0 K. The atomistic simulation technique and modeling tools presented in this study can be used to predict and develop face-centered cubic chemically complex alloys with superior strength for various applications.

Declaration of Competing Interest

None.

Acknowledgments

This research was supported by the U.S. National Science Foundation (DMR- 1807708) and China Scholarship Council (CSC) Fellowship and National Natural Science Foundation of China (11932004).

References

- Z. Wu, H. Bei, G.M. Pharr, E.P. George, Temperature dependence of the mechanical properties of equiatomic solid solution alloys with face-centered cubic crystal structures, Acta Mater. 81 (2014) 428–441.
- [2] M.-H. Tsai, J.-W. Yeh, High-entropy alloys: a critical review, Mater. Res. Lett. 2 (2014) 107–123.
- [3] B. Gludovatz, A. Hohenwarter, D. Catoor, E.H. Chang, E.P. George, R.O. Ritchie, A fracture-resistant high-entropy alloy for cryogenic applications, Science 345 (2014) 1153–1158
- [4] F. Otto, A. Dlouhý, C. Somsen, H. Bei, G. Eggeler, E.P. George, The influences of temperature and microstructure on the tensile properties of a CoCrFeMnNi high-entropy alloy, Acta Mater. 61 (2013) 5743–5755.
- [5] Q. Jiao, G.-D. Sim, M. Komarasamy, R.S. Mishra, P.K. Liaw, J.A. El-Awady, Ther-mo-mechanical response of single-phase face-centered-cubic Al_xCoCrFeNi high-entropy alloy microcrystals, Mater. Res. Lett. 6 (2018) 300–306.
- [6] S. Gangireddy, D. Whitaker, R.S. Mishra, Significant contribution to strength enhancement from deformation twins in thermomechanically processed Al_{0.1}CoCrFeNi microstructures, J. Mater. Eng. Perform. 28 (2019) 1661–1667.
- [7] T.M. Smith, M.S. Hooshmand, B.D. Esser, F. Otto, D.W. McComb, E.P. George, M. Ghazisaeidi, M.J. Mills, Atomic-scale characterization and modeling of 60 dislocations in a high-entropy alloy, Acta Mater. 110 (2016) 352–363.
- [8] S.I. Rao, C. Woodward, T.A. Parthasarathy, O. Senkov, Atomistic simulations of dislocation behavior in a model FCC multicomponent concentrated solid solution alloy, Acta Mater. 134 (2017) 188–194.
- [9] S.I. Rao, C. Varvenne, C. Woodward, T.A. Parthasarathy, D. Miracle, O.N. Senkov, W.A. Curtin, Atomistic simulations of dislocations in a model BCC multicomponent concentrated solid solution alloy, Acta Mater. 125 (2017) 311–320.
- 10] C. Varvenne, A. Luque, W.A. Curtin, Theory of strengthening in fcc high entropy alloys, Acta Mater. 118 (2016) 164–176.

- [11] C. Varvenne, G.P.M. Leyson, M. Ghazisaeidi, W.A. Curtin, Solute strengthening in random alloys. Acta Mater. 124 (2017) 660–683.
- [12] C. Varvenne, A. Luque, W.G. Nohring, W.A. Curtin, Average-atom interatomic potential for random alloys, Phys. Rev. B 93 (2016) 104201.
- [13] F. Maresca, W. Curtin, Mechanistic origin of high strength in refractory BCC high entropy alloys up to 1900K, Acta Mater. 182 (2020) 235–249.
- [14] S.I. Rao, B. Akdim, E. Antillon, C. Woodward, T.A. Parthasarathy, O.N. Senkov, Modeling solution hardening in BCC refractory complex concentrated alloys: NbTiZr, Nb1. 5TiZr0. 5 and Nb0. 5TiZr1. 5, Acta Mater. 168 (2019) 222–236.
- [15] S.I. Rao, E. Antillon, C. Woodward, B. Akdim, T.A. Parthasarathy, O.N. Senkov, Solution hardening in body-centered cubic quaternary alloys interpreted using Suzuki's kink-solute interaction model, Script. Mater. 165 (2019) 103–106.
- [16] S. Plimpton, Fast parallel algorithms for short-range molecular dynamics, J. Comput. Phys. 117 (1995) 1–19.
- [17] X.W. Zhou, H.N.G. Wadley, R.A. Johnson, D.J. Larson, N. Tabat, A. Cerezo, A.K. Petford-Long, G.D.W. Smith, P.H. Clifton, R.L. Martens, T.F. Kelly, Atomic scale structure of sputtered metal multilayers, Acta Mater. 49 (2001) 4005–4015.
- [18] P.M. Anderson, J.P. Hirth, J. Lothe, Theory of Disloactions, third ed., Cambridge University Press, 2017.
- [19] L. Ventelon, F. Willaime, Generalized stacking-faults and screw-dislocation core-structure in bcc iron: A comparison between ab initio calculations and empirical potentials, Phil.Mag. 90 (2010) 1063–1074.
- [20] D. Farkas, A. Caro, Model interatomic potentials and lattice strain in a high-entropy alloy, J. Mat. Res. 33 (2018) 3218–3225.
- [21] D. Faken, H. Jónsson, Systematic analysis of local atomic structure combined with 3D computer graphics, Comput. Mater. Sci. 2 (1994) 279–286.
- [22] A. Stukowski, Visualization and analysis of atomistic simulation data with OVI-TO-the Open Visualization Tool, Modell. Simul. Mater. Sci. Eng. 18 (2010) 015012.
- [23] F. Tian, L.K. Varga, N. Chen, J. Shen, L. Vitos, Empirical design of single phase high-entropy alloys with high hardness, Intermetallics 58 (2015) 1–6.

- [24] F. Mouhat, F.-X. Coudert, Necessary and sufficient elastic stability conditions in various crystal systems, Phys. Rev. B Condens. Matter 90 (2014) 224104.
- [25] M.J. Mehl, J.E. Osburn, D.A. Papaconstantopoulos, B.M. Klein, Structural properties of ordered high-melting-temperature intermetallic alloys from first-principles total-energy calculations, Phys. Rev. B Condens. Matter 41 (1990) 10311–10323.
- [26] J.M.J. den Toonder, J.A.W. van Dommelen, F.P.T. Baaijens, The relation between single crystal elasticity and the effective elastic behaviour of polycrystalline materials: theory, measurement and computation, Modell. Simul. Mater. Sci. Eng. 7 (1999) 909–928.
- [27] G. Laplanche, A. Kostka, C. Reinhart, J. Hunfeld, G. Eggeler, E.P. George, Reasons for the superior mechanical properties of medium-entropy CrCoNi compared to highentropy CrMnFeCoNi, Acta Mater. 128 (2017) 292–303.
- [28] A.J. Zaddach, C. Niu, C.C. Koch, D.L. Irving, Mechanical properties and stacking fault energies of NiFeCrCoMn high-entropy alloy, JOM 65 (2013) 1780–1789.
- [29] M.C. Gao, J.-W. Yeh, P.K. Liaw, Y. Zhang, High-Entropy Alloys: Fundamentals and Applications, Springer, 2016.
- [30] J.P. Hirth, J. Lothe, Theory of dislocations, 2nd., Wiley, 1982.
- [31] C.R. LaRosa, M. Shih, C. Varvenne, M. Ghazisaeidi, Solid solution strengthening theories of high-entropy alloys, Mater. Charact. 151 (2019) 310–317.
- [32] Y. Zhang, T. Zuo, Y. Cheng, P.K. Liaw, High-entropy alloys with high saturation magnetization, electrical resistivity, and malleability, Sci. Rep. 3 (2013) 1455.
- [33] L. Liu, J.B. Zhu, C. Zhang, J.C. Li, Q. Jiang, Microstructure and the properties of FeCoCuNiSnx high entropy alloys, Mater. Sci. Eng. A 548 (2012) 64–68.
- [34] W.H. Liu, Y. Wu, J.Y. He, T.G. Nieh, Z.P. Lu, Grain growth and the Hall–Petch relationship in a high-entropy FeCrNiCoMn alloy, Script. Mater. 68 (2013) 526–529.
- [35] J. Ding, Q. Yu, M. Asta, R.O. Ritchie, Tunable stacking fault energies by tailoring local chemical order in CrCoNi medium-entropy alloys, Proc. Natl. Acad. Sci 115 (2018) 8919–8924.
- [36] Q. Li, H. Sheng, E. Ma, Strengthening in multi-principal element alloys with localchemical-order roughened dislocation pathways, Nat. Commun. 10 (2019) 3563.